The Journal of Chemical Physics

Multi-level quantum Rabi model for anharmonic vibrational polaritons

Cite as: J. Chem. Phys. **151**, 144116 (2019); https://doi.org/10.1063/1.5121426
Submitted: 24 July 2019 . Accepted: 09 September 2019 . Published Online: 14 October 2019

Federico J. Hernández, and Felipe Herrera

COLLECTIONS

Note: This paper is part of the JCP Emerging Investigators Special Collection.

This paper was selected as an Editor's Pick

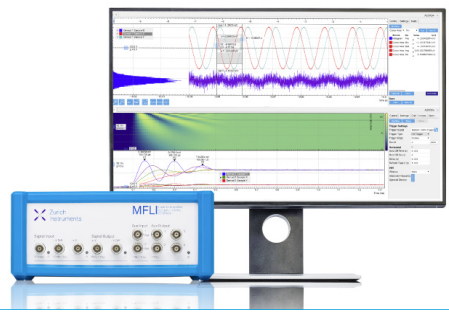

The Journal of Chemical Physics ARTICLE scitation.org/journal/jcp

Multi-level quantum Rabi model for anharmonic vibrational polaritons

Cite as: J. Chem. Phys. 151, 144116 (2019); doi: 10.1063/1.5121426
Submitted: 24 July 2019 • Accepted: 9 September 2019 •
Published Online: 14 October 2019

Federico J. Hernández[1] and Felipe Herrera[1,2,a)]

AFFILIATIONS

[1] Department of Physics, Universidad de Santiago de Chile, Av. Ecuador, 3493 Santiago, Chile
[2] Millennium Institute for Research in Optics MIRO, Concepción, Chile

Note: This paper is part of the JCP Emerging Investigators Special Collection.
[a)] **Electronic mail:** felipe.herrera.u@usach.cl

ABSTRACT

We propose a cavity QED approach to describe light-matter interaction of an infrared cavity field with an anharmonic vibration of a single nonpolar molecule. Starting from a generic Morse oscillator potential with quantized nuclear motion, we derive a multilevel quantum Rabi model to study vibrational polaritons beyond the rotating-wave approximation. We analyze the spectrum of vibrational polaritons in detail and compare it with available experiments. For high excitation energies, the system exhibits a dense manifold of polariton level crossings and avoided crossings as the light-matter coupling strength and cavity frequency are tuned. We also analyze polariton eigenstates in nuclear coordinate space. We show that the bond length of a vibrational polariton at a given energy is never greater than the bond length of a Morse oscillator with the same energy. This type of polariton bond strengthening occurs at the expense of the creation of virtual infrared cavity photons and may have implications in chemical reactivity of polariton states.

I. INTRODUCTION

Cavity quantum electrodynamics (QED) has been intensely studied for the development of quantum technology over the last decade.[1,2] Precision experiments under carefully controlled conditions have been implemented to achieve conditions under which quantum optical effects become relevant in applications.[3–5] Chemical systems and molecular materials at ambient conditions for long have been considered to be unnecessarily complex and uncontrollable to enable useful quantum optical effects. In recent years, the demonstration of reversible modifications of chemical properties in molecular materials via strong coupling (SC) to confined light has extended the study of cavity QED as an emerging research in chemical physics.[6] Light-matter interaction in the strong coupling (SC) and ultrastrong coupling (USC) regimes opens the possibility of creating novel hybrid photon-molecule states whose unique properties may enable novel applications in chemistry and material science.

In the infrared regime, the coupling of an intramolecular vibration to the quantized electromagnetic vacuum of a Fabry-Pérot cavity can lead to the formation of vibrational polaritons.[7–21] These hybrid light-matter states exhibit fundamentally novel properties in comparison with free-space vibrations. For instance, vibrational polaritons may enable the selective control of chemical reactions,[21–23] a long-standing goal in physical chemistry.[24] Strong light-matter coupling provides a reversible way of modifying reactive processes without changing the chemical composition of materials and also modifies the radiative and nonradiative dynamics of molecular vibrations.[25–31] Several recent studies on vibrational strong coupling (VSC) within the ground electronic state have shown that chemical reactions can proceed through novel pathways in comparison with free space. Under VSC, reactions may be inhibited or catalyzed, or the product branching ratios may be tilted.[7,16,22,23] For instance, by strongly coupling the carbon-silyl (Si–C) bond stretching vibration of 1-phenyl-2-trimethylsilylacetylene to the electromagnetic vacuum of a resonant infrared microfluidic cavity, the rate of Si—C bond breakage has been shown to decrease by a moderate factor of order unity.[16] In another recent study,[22] the catalytic effect of VSC on the hydrolysis of cyanate ions and ammonia borane, under coupling of a Fabry-Pérot cavity with the

broad OH infrared absorption band of water, was demonstrated. The measured increase in the reaction rate constant by two orders of magnitude relative to free space for cyanate and by four orders of magnitude for ammonia borane is one of the first reports of cavity-enhanced reactivity, a possibility earlier predicted for electron transfer reactions in microcavities.[32] In another study, very precise chemical control was carried out on a compound having two available silyl bond cleavage sites, Si—O and Si—C. For this system, simultaneous VSC with three spectrally distinct vibrational modes was shown to modify the reactivity landscape such that the branching ratio of Si—C and Si—O cleavage was altered by simply tuning the cavity resonance conditions.[23]

The diverse experimental evidence on VSC represents a challenge for theoretical modeling, mainly due to the inherent complexity of potential energy landscapes of reactive species, as well as collective effects that are relevant in molecular ensembles. Despite recent theoretical progress,[14,28,31,33–40] it remains unclear whether there is a universal mechanism for the modification of ground state (GS) chemical reactivity under VSC or the problem is system-specific. Common explanations for experimental observations are based on traditional chemical concepts such as changes in the potential energy surface, modifications of an activation energy, or changes in the relative energy of reactants and products. However, as we discuss throughout, under VSC, it is difficult to justify the conventional physical meaning assigned to these traditional concepts.

In this work, we introduce a cavity QED approach to study anharmonic vibrational polaritons in the single-molecule limit. The method describes the molecular subsystem as an individual anharmonic IR-active vibrational mode with quantized nuclear motion, as illustrated in Fig. 1. We focus on molecules without permanent dipole in equilibrium. This type of molecular species has been studied before in IR cavities: carbonyl asymmetric stretching in $Fe(CO)_5$[14] and $W(CO)_6$,[26,27,41] and C=S asymmetric stretching of CS_2.[14]

The vibrational mode interacts with a vacuum field via electric dipole coupling. Discrete-variable representation (DVR) is used to describe the cavity-free anharmonic vibration, and the electric dipole interaction is treated with a cavity QED approach that includes counter-rotating terms. This total system Hamiltonian corresponds to a multilevel quantum Rabi (MLQR) model. By construction, vibrational polariton states can be analyzed in Hilbert space and also in coordinate space. The method can be scaled to the many-molecule regime.

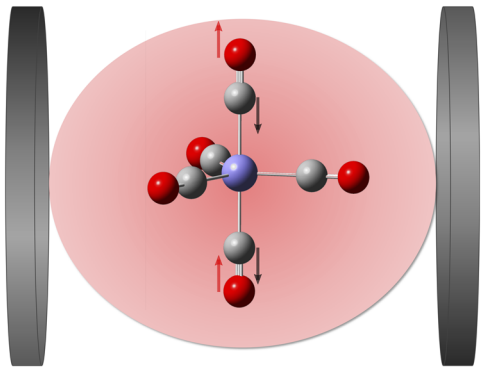

FIG. 1. Schematic diagram of a single $Fe(CO)_5$ molecule coupled to the quantized electromagnetic vacuum of an infrared Fabry-Pérot cavity. The arrows represent the nuclei displacements in a carbonyl asymmetric stretching mode.

The rest of the article is organized as follows: In Sec. I, we review the properties of Morse oscillators. The construction of the multilevel quantum Rabi model is discussed in Sec. II. In Sec. III, we describe the spectrum of vibrational polaritons arising from the model. In Sec. IV, we analyze the representation of vibrational polaritons in nuclear coordinate space. In Sec. V, we analyze the level crossings that occur in the excited polariton manifold. We conclude and discuss future developments in Sec. VI.

II. MORSE OSCILLATOR

We model the nuclear motion of an anharmonic nonpolar vibration with a Morse potential[42]

$$V(q) = D_e(1 - \exp[-a(q - q_e)])^2, \tag{1}$$

where D_e is the classical dissociation energy (without zero point motion), q_e is the equilibrium bond length, and a is a parameter. The vibrational Schrödinger equation with a Morse potential can be solved analytically in terms of associated Laguerre polynomials[42,43] or numerically using grid-based methods.[44] We use DVR on a uniform grid with Fourier basis functions[45] to obtain the vibrational wavefunctions and eigenvalues of the Morse potential. For the dimensionless parameters $D_e = 12.0$, $q_e = 4.0$, and $a = 0.2041$, the corresponding potential is shown in Fig. 2(a). For the dimensionless mass $\mu = 1$, this potential has 24 bound states in agreement with Ref. 46 and is used throughout. In the supplementary material, we show that our conclusions do not vary qualitatively for other values of a and μ, with fixed D_e. Our results also qualitatively hold for other values of D_e, provided the number of Morse bound states still exceeds the maximum vibrational level that significantly contributes to the vibrational polariton spectrum within the energy range considered in this work.

As we explain below, the degree of anharmonicity in the potential has a profound effect in the behavior of vibrational polaritons. For the Morse potential, the anharmonicity can be easily tuned by changing the parameters a and μ, for fixed binding energy D_e. The relation between these parameters and the degree of anharmonicity can be understood from the exact eigenvalues of the Morse Hamiltonian,[42]

$$E_v = -D_e + \hbar a\sqrt{\frac{2D_e}{\mu}}\,(v + 1/2) - \frac{\hbar^2 a^2}{2\,\mu}(v + 1/2)^2, \tag{2}$$

where v is the vibrational quantum number. By comparing this expression with the Dunham expansion,[47]

$$E_v = Y_{00} + \omega_0(v + 1/2) - \omega_0\chi_e(v + 1/2)^2 + \ldots, \tag{3}$$

where ω_0 is the vibrational frequency, the anharmonic coefficient χ_e can be written as

$$\chi_e = \frac{\hbar^2 a\pi}{(2\mu D_e)^{1/2}}. \tag{4}$$

Vibrations with lower μ and higher a therefore have stronger spectral anharmonicity, for fixed dissociation energy. We illustrate

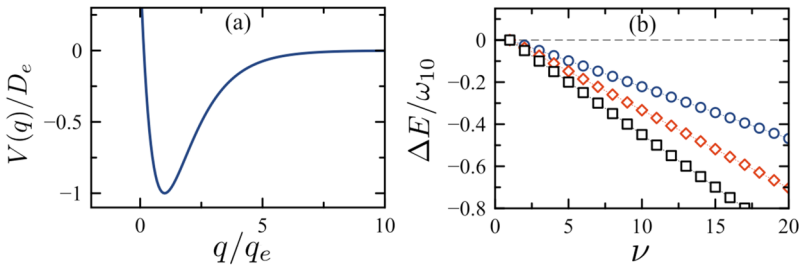

FIG. 2. (a) Morse potential $V(q)$, in units of the classical dissociation energy D_e. We use $D_e = 12$, $q_e = 4$, $a = 0.204$ (dimensionless) to generate 24 bound states. (b) Anharmonicity of the energy spacing between adjacent Morse eigenstates $\Delta E \equiv \omega_{\nu,\nu-1} - \omega_{10}$. We use $D_e = 12.0$, $q_e = 4.0$ for all points, with $\mu = 3$ and $a = 0.204$ (circles), $\mu = 1$ and $a = 0.175$ (diamonds), and $\mu = 1$ and $a = 0.233$ (squares). The dashed line is the harmonic oscillator limit ($\Delta E = 0$).

this dependence in Fig. 2(b), where the change in the vibrational energy level spacing relative to the fundamental frequency ω_{10} for $\nu = 1 \leftarrow \nu = 0$ is shown for different values of μ and a. The level spacing between adjacent vibrational states can be significantly smaller than the harmonic oscillator value ω_{10}, even for relatively low values of ν.

The electronic wavefunction determines the contribution to the molecular dipole moment of the electron charge distribution, which in the Born-Oppenheimer approximation is a parametric function $d(\{\mathbf{q}\})$ of all nuclear coordinates $\{\mathbf{q}\}$. In general, the dipole function $d(\{\mathbf{q}\})$ can be obtained using *ab initio* quantum chemistry for simple molecular species. Since we are interested in understanding universal features of nonpolar anharmonic vibrational polaritons, we adopt a model functional form $d(q)$ that captures the correct physical behavior of an individual anharmonic IR-active vibrational mode without permanent dipole moment. (i) The function must be continuous over the entire range of q; (ii) its value at the equilibrium distance must be zero; (iii) the function must have a maximum at some finite value of q; and (iv) the function must asymptotically vanish as the neutral bond dissociates into neutral species. These requirements are satisfied by the following function:

$$d(q) = (q - c_0)\exp\left[-(q - c_1)^2/\sigma^2\right], \tag{5}$$

which we show in Fig. 3(a) for $c_0 = c_1 = q_e$ and $\sigma = 0.5q_e$. c_0 is the coordinate at which $d(q) = 0$; σ and c_1 control the location and magnitude of the maximum and minimum values of the dipole function, also its behavior far from the equilibrium distance. For $c_1 = q_e$, the function $d(q)$ is symmetric with respect to q_e [as in Fig. 3(a)]. For $c_1 > q_e$, the maximum dipole moment moves to higher values of q and the function $d(q)$ becomes asymmetric around q_e.

In order to describe light-matter coupling properly, we need a reasonable description of the electric dipole moment not only near the equilibrium distance q_e but also in the long range up to the dissociation threshold. This is because strong light-matter coupling in a cavity can strongly admix several vibrational eigenstates with high ν. Furthermore, we are interested in studying how highly exited polaritons behave near the energy dissociation threshold of the free-space molecular subsystem. Therefore, dipole matrix elements between all bound and unbound states of the Morse potential must be accurately estimated. In Figs. 3(b) and 3(c), we show the scaling with ν of the diagonal and off-diagonal vibrational dipole matrix elements. The permanent dipole moments $\langle\nu|\hat{d}(q)|\nu\rangle$ decrease in magnitude with ν [panel 3(b)], as expected from the behavior of $d(q)$ on a neutral Morse oscillator. This trend also holds for different values of a and μ in the Morse potential. The higher the oscillator's mass, the lower the rate of decrease of the permanent dipoles. Figure 3(c) shows that for a fixed vibrational eigenstate $|\nu'\rangle$, the transition dipole moments with neighboring states $|\nu\rangle$ ($\nu \neq \nu'$) cannot be ignored and must be taken into account in the light-matter coupling.

In linear infrared absorption of high-frequency modes (e.g., $\omega_{10} \approx 1700\ \mathrm{cm}^{-1}$ for carbonyl stretching), only the ground vibrational level $\nu = 0$ is populated at room temperature ($kT/\hbar\omega_{10} \ll 1$). The oscillator strength of the fundamental absorption peak ($\nu = 0 \rightarrow 1$) and its overtones ($|\Delta\nu| \geq 2$) are thus proportional to $|\langle\nu|\hat{d}(q)|0\rangle|^2$ with $\nu \geq 1$. Figure 3(c) (circles) captures the typical IR absorption pattern of decreasing overtone strength for higher $\Delta\nu$.[48] This qualitatively correct behavior validates the dipole model function $d(q)$ in Eq. (5).

Using strong infrared laser pulses, it is possible to prepare vibrational modes with high quantum numbers $\nu \gg 1$, even when

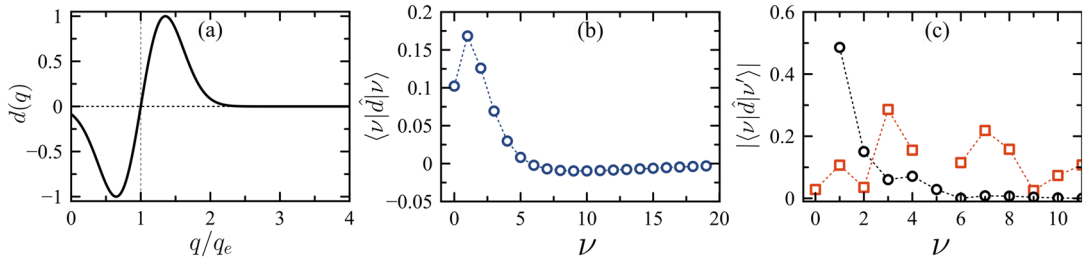

FIG. 3. (a) Model electric dipole function $d(q)$ for the vibrational mode of an IR-active nonpolar molecule [$d(q_e) = 0$], normalized to its maximum value. (b) Permanent dipole moment matrix elements $\langle\nu|d(q)|\nu\rangle$ as a function of the vibrational quantum number ν. (c) Dipole matrix elements $\langle\nu|d(q)|\nu'\rangle$ as a function of ν, for $\nu' = 0$ (circles) and $\nu' = 5$ (squares). Dipole matrix elements are normalized to the maximum of $d(q)$. The dipole function parameters used are $c_0 = c_1 = 4$ and $\sigma = 2$. The Morse parameters used are $D_e = 12.0$, $q_e = 4.0$, $a = 0.204$, and $\mu = 1$.

$kT/\hbar\omega_{10} \ll 1$. This off-resonant driving is known as vibrational ladder climbing and has been used in nonlinear spectroscopic measurements.[49] Vibrational ladder climbing is determined by the matrix elements $\langle v|\hat{d}|v'\rangle$ with $v' \neq v \geq 1$, corresponding to dipole transitions between overtones. Figure 3(c) (squares) shows that these high-v matrix elements can be as strong as the first overtones of the fundamental transition (circles), over a range of neighboring levels with $|v - v'| \leq 4$, for our choice of $d(q)$. We show below that ignoring dipole couplings between high-v overtones fails to describe the rich and complex physics of the excited polariton manifold up to the dissociation threshold. Excited polariton levels can be expected to be relevant in the description of nonlinear cavity transmission signals, chemical reactions, and heat transport.

III. MULTILEVEL QUANTUM RABI MODEL

We derive the total Hamiltonian for the molecule-cavity system starting using the Power-Zineau-Woolley (PZW) multipolar formulation of light-matter interaction.[50] The PZW frame is equivalent to minimal-coupling by a unitary transformation that eliminates the vector potential $\mathbf{A}(\mathbf{x})$ from the Hamiltonian.[50] We divide the total Hamiltonian $\hat{\mathcal{H}}$ in the three terms of the form $\hat{H} = \hat{H}_{\rm M} + \hat{H}_{\rm C} + \hat{H}_{\rm LM}$. The molecular part is given by

$$\hat{H}_{\rm M} = \hat{H}_{\rm el} + \hat{H}_{\rm nuc} + \int d\mathbf{x}\, |\mathbf{P}(\mathbf{x})|^2, \tag{6}$$

where the first two terms correspond to the electronic and nuclear Hamiltonians in the Born-Oppenheimer approximation, and the third term is the dipole self-energy, with $\mathbf{P}(\mathbf{x})$ being the macroscopic polarization density. We follow the approach in Refs. 51 and 52, where the dipole self-energy is shown to result in energy shifts that can be formally absorbed into $\hat{H}_{\rm el}$. This should be compared with Refs. 39 and 53, in which an explicit quadratic dependence on charge coordinates is kept in $\hat{H}_{\rm M}$.

The nuclear Hamiltonian $\hat{H}_{\rm nuc}$ in Eq. (6) in general describes not only vibrational motion but also molecular rotations. Since we are interested in condensed-phase vibrational polaritons, we assume that molecular rotations are slower than the time scale for polariton formation and only represent additional contributions to the vibrational absorption linewidth.[54]

The free cavity Hamiltonian $\hat{H}_{\rm C}$ is given by

$$\begin{aligned}\hat{H}_{\rm C} &= \frac{1}{2}\int d\mathbf{x}\left(|\mathbf{D}(\mathbf{x})|^2 + \frac{1}{\mu_0}|\mathbf{H}(\mathbf{x})|^2\right)\\ &= \sum_\xi \hbar\omega_\xi\left(\hat{a}_\xi^\dagger\hat{a}_\xi + 1/2\right),\end{aligned} \tag{7}$$

where $\mathbf{D}(\mathbf{x})$ and $\mathbf{H}(\mathbf{x})$ are the macroscopic displacement and magnetic fields, respectively. μ_0 is the magnetic permeability. In the second line, we imposed canonical field quantization into a set of normal modes with continuum label ξ, frequencies ω_ξ, and annihilation operators $\hat{a}_\xi$. Light-matter interaction in the PZW frame, ignoring magnetic moments, is given by[50]

$$\hat{H}_{\rm LM} = \int d\mathbf{x}\, \mathbf{P}(\mathbf{x})\cdot\mathbf{D}(\mathbf{x}). \tag{8}$$

The solutions of the electronic Hamiltonian $\hat{H}_{\rm el}$ are assumed to be known within the Born-Oppenheimer approximation such that they give the dipole function $d(q)$. We adopt a point-dipole approximation for the polarization density, i.e., $\mathbf{P}(\mathbf{x}) = \mathbf{d}\,\delta(\mathbf{x} - \mathbf{x}_0)$, where $\mathbf{d}$ is the electric dipole vector and $\mathbf{x}_0$ is the location of the molecule.

We adopt a single-mode approximation for the cavity Hamiltonian in Eq. (7) by setting $\omega_\xi \equiv \omega_c$ for all ξ and define the effective field operator $\hat{a} = \sum_\xi \hat{a}_\xi$ (up to a normalization constant). This simplification is justified in Fabry-Pérot cavities with a large free-spectral range (FSR ~ 300–500 $\rm cm^{-1}$[9]) and low transmission linewidths (FWHM ~ 10–40 $\rm cm^{-1}$[9]). In this approximation, the intracavity displacement field operator can be approximated by $\hat{\mathbf{D}} \approx \mathcal{E}_0(\hat{a} + \hat{a}^\dagger)$, where $\mathcal{E}_0$ can be considered as the amplitude of the vacuum field fluctuations or the electric field per photon (ignoring vectorial character). $\mathcal{E}_0$ scales as $1/\sqrt{V_m}$ with the effective cavity mode volume V_m.[55] We thus write the light-matter interaction term as

$$\hat{H}_{\rm LM} = \mathcal{E}_0\,(\hat{d}_+ + \hat{d}_-) \otimes (\hat{a} + \hat{a}^\dagger), \tag{9}$$

where the up-transition operator $\hat{d}_+$ projected into the vibrational energy basis $|v\rangle$ is given by

$$\hat{d}_+ = \sum_{v,v'>v} \langle v'|d(q)|v\rangle |v'\rangle\langle v|, \tag{10}$$

with $\hat{d}_- = (\hat{d}_+)^\dagger$. Permanent dipole moments are found to give negligible contributions for the range of light-matter couplings considered. By combining Eqs. (6), (7), and (9), we arrive at the total system Hamiltonian

$$\hat{\mathcal{H}} = \omega_c\,\hat{a}^\dagger\hat{a} + \sum_v \omega_v |v\rangle\langle v| + \sum_v \sum_{v'>v} g_{v'v}(|v'\rangle\langle v| + |v\rangle\langle v'|)(\hat{a} + \hat{a}^\dagger), \tag{11}$$

where ω_v is the energy of the vibrational eigenstate $|v\rangle$, and $g_{v'v} = \mathcal{E}_0\langle v'|d(q)|v\rangle$ for $v' > v$ is a state-dependent Rabi frequency. The zero of energy is defined by the energy of the vibrational ground state ($v = 0$) in the cavity vacuum. Equation (11) corresponds to a multilevel quantum Rabi (MLQR) model, which reduces to the quantum Rabi model for a two-level system,[56–58] when the vibrational subspace is truncated to $v = 0$, 1 and the energy reference is rescaled.

The vacuum field amplitude $\mathcal{E}_0$ is considered here as a tunable parameter that determines the light-matter coupling strength. In a cavity with small mode volume, the mode amplitude $\mathcal{E}_0$ can be large and tunable by fabrication.[12] Moreover, the cavity detuning $\Delta \equiv \omega_c - \omega_{10}$ is another energy scale that can be tuned by fabrication.

For convenience, we define the state-independent Rabi frequency

$$g \equiv g_{10} = \mathcal{E}_0\,\langle 1|d(q)|0\rangle. \tag{12}$$

Although we use the single parameter g to quantify light-matter coupling strength throughout, we emphasize that dipole transitions $v \leftrightarrow v'$ in Eq. (11) have in general different coupling strengths. As we show below, due to the multilevel nature of the molecular emitter, counter-rotating terms in Eq. (11) start to become relevant in the polariton spectrum for values of g/ω_{10} that would still be considered within the rotating-wave approximation for the qubit.[31]

IV. SPECTRUM OF VIBRATIONAL POLARITONS

In order to gain some physical intuition about the structure of vibrational polaritons, in Fig. 4, we illustrate thelight-matter

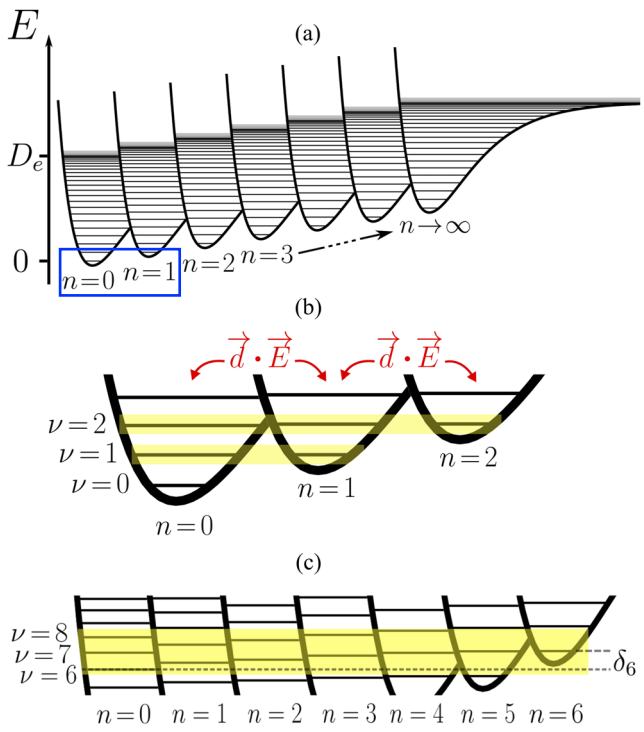

FIG. 4. (a) Illustration of resonant light-matter coupling between a Morse oscillator with dissociation energy D_e and a quantized cavity field with photon number n (unbound). Each Morse potential corresponds to the uncoupled subspace $|v\rangle|n\rangle$. (b) Low energy couplings involving the subspace $\mathcal{S}_1 = \{|1\rangle|0\rangle, |0\rangle|1\rangle\}$ at $E \approx \omega_{10}$, and $\mathcal{S}_2 = \{|2\rangle|0\rangle, |1\rangle|1\rangle, |0\rangle|2\rangle\}$ at $E \approx 2\omega_{10}$. Dipole coupling within $\mathcal{S}_1$ leads to the formation of the lower and upper polaritons, and coupling within $\mathcal{S}_2$ leads to the formation of a polariton triplet. (c) High energy couplings involving $\mathcal{S}_6$ at $E \approx 6\omega_{10}$. State $|6\rangle|0\rangle$ is red shifted with respect to $|0\rangle|6\rangle$ by δ_6, for $\omega_{10} = \omega_c$. The highlighted levels can strongly admix.

coupling scheme implied by the uncoupled basis $|v\rangle|n\rangle$, where $|n\rangle$ is a cavity Fock state. We can associate a complete vibrational manifold $\{|v\rangle; v = 0, 1, 2, \ldots\}$ to every Fock state of the cavity $|n\rangle$. The ground level in each vibrational manifold ($v = 0$) has energy $n\omega_c$ in the Fock state $|n\rangle$, and the dissociation energy E_∞ becomes

$$E_\infty = D_e + n\omega_c. \tag{13}$$

Only in the cavity vacuum ($n = 0$), the bond dissociation energy coincides with the value expected for a Morse oscillator in free space. In general, the energy required to break a chemical bond depends on the quantum state of the cavity field.

Vibrational manifolds with different Fock states can couple each other via the light-matter term in Eq. (9). Since parity is broken for vibrational states due to anharmonicity, the only quasi-selection rule that holds is $\Delta n = \pm 1$ because the free cavity Hamiltonian $\hat{H}_C$ commutes with parity. Therefore, vibrational states $|v\rangle$ and $|v'\rangle$ that differ by one photon number can admix due to light-matter coupling. Because of anharmonicity, admixing of vibrational states with $|v - v'| \geq 1$ is allowed. The amount of admixing that can occur between vibrational eigenstates in different manifolds is ultimately determined by the electric dipole function $d(q)$.

The number of bare states $|v\rangle|n\rangle$ that can potentially admix to form vibrational polariton eigenstates grows as the total energy increases. Throughout this work, we include all vibrational and Fock basis states that are necessary to converge the polariton spectrum up to a given energy of interest $E < D_e$. Figure 4(b) shows that for the lowest Fock states, resonant coupling at energy $E \approx \omega_{10}$ only involves the subspace $\mathcal{S}_1 = \{|1\rangle|0\rangle, |0\rangle|1\rangle\}$ for $g/\omega_{10} \ll 1$. This coupling results in the formation of the so-called lower polariton (LP) and upper polariton (UP), which are observable in linear spectroscopy.[6,9] They can be written as

$$|\Psi_1\rangle = \alpha|0\rangle|1\rangle - \beta|1\rangle|0\rangle, \tag{14a}$$

$$|\Psi_2\rangle = \beta|0\rangle|1\rangle + \alpha|1\rangle|0\rangle, \tag{14b}$$

where $|\Psi_1\rangle$ and $|\Psi_2\rangle$ correspond to LP and UP, respectively. The orthonormal coefficients α and β depend on g and Δ. $|\Psi_1\rangle$ and $|\Psi_2\rangle$ in Eq. (14) coincide with the first excitation manifold of the Jaynes-Cummings model.[59] Figure 4(b) also shows that for $g/\omega_{10} \ll 1$, resonant coupling at energy $E \approx 2\omega_{10}$ only involves the subspace $\mathcal{S}_2 = \{|2\rangle|0\rangle, |1\rangle|1\rangle, |0\rangle|2\rangle\}$, leading to the formation of three polariton branches, as discussed below. For $g/\omega_{10} \sim 0.1$, coupling of bare states $|v\rangle|n\rangle$ beyond $\mathcal{S}_1$ and $\mathcal{S}_2$ is allowed by counter-rotating terms in Eq. (9).

In Fig. 4(c), we consider the coupling between vibrational manifolds around energy $E \approx 6\ \omega_{10}$. If the molecular vibrations were harmonic, vibrational states $|v\rangle$ would have energy $v\omega_{10}$. Due to anharmonicity, vibrational levels in free space have energy

$$\omega_v = v\,\omega_{10} - \delta_v,$$

where $\delta_v > 0$ is the shift from a harmonic oscillator level, shown in Fig. 2 for a Morse oscillator. For $v = 6$, the anharmonic shift δ_6 is not negligible in comparison with ω_{10}, which means that for the smaller couplings $g/\omega_{10} \ll 1$, the number of bare states $|v\rangle|n\rangle$ that can resonantly admix is relatively limited. This resembles the role of anharmonicity in limiting the efficiency of vibrational ladder climbing using laser pulses.[49,60]

On the other hand, Fig. 4(c) suggests that for larger coupling ratios g/ω_{10}, there is a greater number of quasidegenerate bare states $|v\rangle|n\rangle$ that are energetically available to admix within an energy range 2δ. As the total energy increases, the density of quasidegenerate bare states that can strongly admix within a bandwidth δE grows. We show below that this complex coupling structure leads to a large density of true and avoided crossings in the excited polariton manifold, even for relatively low values of the coupling ratio g/ω_{10}.

In Fig. 5, we show the spectrum of anharmonic vibrational polaritons as a function of g and Δ. Figure 5(a) shows that the system has a unique nondegenerate ground state $|\Psi_0\rangle$ (GS). The first excited manifold features a LP-UP doublet that scales linearly with g over the range of couplings considered ($R^2 = 1.000$ for log-log fit). However, the LP-UP splitting is not symmetric around $E = \omega_{10}$, which is the energy of the degenerate bare states $|1\rangle|0\rangle$ and $|0\rangle|1\rangle$ for $\omega_c = \omega_{10}$. Figure 5(a) shows the polariton triplet around $E = 2\omega_{10}$, associated with light-matter coupling within the subspace $\mathcal{S}_2$ discussed above [see Fig. 4(b)]. Multiple true and avoided crossings occur at energies $E \geq 2\omega_{10}$ over the entire range of couplings considered. The density of energy crossings grows with increasing energy.

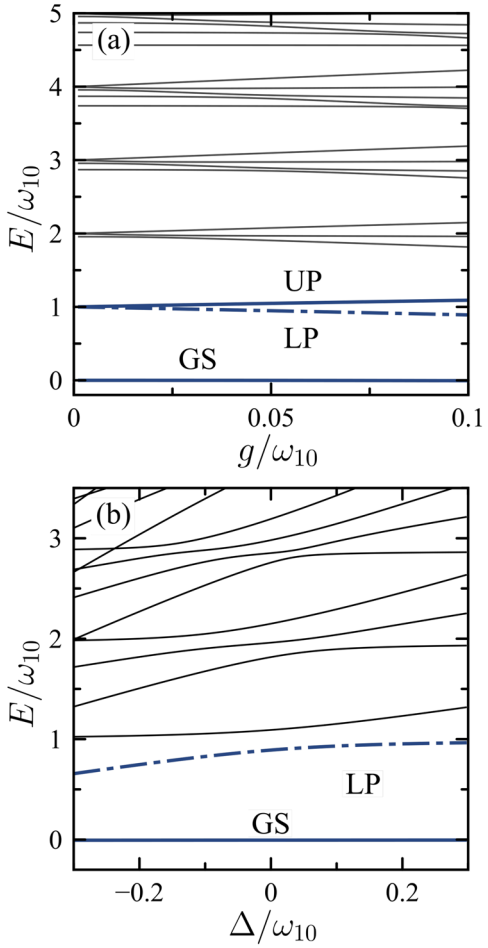

FIG. 5. (a) Spectrum of anharmonic vibrational polaritons as a function of the coupling strength g/ω_{10}, for resonant coupling $\omega_c = \omega_{10}$. The ground state (GS), lower (LP), and upper (UP) are highlighted. (b) Vibrational polariton spectrum as a function of the cavity detuning from the fundamental frequency $\Delta = \omega_c - \omega_{10}$. The GS and LP are highlighted. We set $g = 0.1\omega_{10}$. Energy is in units of ω_{10}.

In Fig. 5(b), we show the polariton spectrum as a function of detuning $\Delta \equiv \omega_c - \omega_{10}$, for $g/\omega_{10} = 0.1$. Several true and avoided crossings develop in the excited manifold. When $\Delta \sim g$, the energetic ordering of the excited polaritons can change in comparison with the resonant regime ($\Delta/g \ll 1$). For example, there is an avoided crossing at $E \approx 1.9\ \omega_{10}$ near $\Delta \approx 0.05\ \omega_{10}$. The 5th and 6th excited polaritons develop a true crossing at $\Delta \approx -0.3\ \omega_{10}$. This raises concerns regarding the assignment of spectral lines in linear and nonlinear cavity transmission spectroscopy for light-matter coupling in the dispersive regime $|\Delta|/g \gtrsim 1$.

V. VIBRATIONAL POLARITONS IN NUCLEAR COORDINATE SPACE

In molecules and materials, the strength of a chemical bond is commonly associated with its vibration frequency ω_0 via the relation

$$\omega_0 = \sqrt{k/\mu}, \tag{15}$$

where k is the bond spring constant and μ is the reduced mass of the vibrating nuclei. Stronger bonds (higher k) thus lead to higher vibrational frequencies. This simple argument has also been used to discuss the bonding character of vibrational polaritons under strong coupling.[6] In this section, we show that the description of the bonding strength of vibrational polaritons is far more complex than the commonly used spring model suggests.

In order to analyze vibrational polaritons in nuclear coordinate space, keeping photons in Hilbert space, let us expand the eigenstates of Eq. (11) in the uncoupled basis $\{|v\rangle|n\rangle\}$ as

$$|\Psi_j\rangle = \sum_{v,n} c^j_{vn}|v\rangle|n\rangle, \tag{16}$$

where c^j_{vn} are orthonormal coefficients associated with the jth eigenstate. We can rewrite Eq. (16) by combining vibrational components associated with a given photon number n as

$$|\Psi_j\rangle = \sum_{n} |\Phi^j_n\rangle|n\rangle, \tag{17}$$

where $|\Phi^j_n\rangle = \sum_v c^j_{vn}|v\rangle$. The state $|\Phi^j_n\rangle$ can be interpreted as a vibrational wave packet conditional on the cavity photon number. Its nuclear coordinate representation is simply given by the projection

$$\Phi_{jn}(q) = \langle q|\Phi^j_n\rangle. \tag{18}$$

For concreteness, we show in Fig. 6 a set of normalized conditional probability distributions $|\Phi_{jn}(q)|^2$ with $n \le 4$, for the excited polariton eigenstate $|\Psi_6\rangle$ under resonant light-matter coupling. Since the energy of excited polariton $|\Psi_6\rangle$ tends asymptotically to $E_6 \approx 3\ \omega_{10}$ as $g \to 0$, one could expect the normalized probability distribution $|\Phi_{6n}(q)|^2$ to resemble the behavior of the Morse oscillator eigenfunction with $v = 3$ for $g/\omega_{10} \ll 1$. Figure 6 (lower panel) shows that indeed the vacuum component ($n = 0$) of $|\Psi_6\rangle$ qualitatively matches the node structure of the bare Morse oscillator state $|v = 3\rangle$ for $g/\omega_{10} = 0.1$.

Figure 6 also shows that the nuclear densities $|\Phi_{6n}(q)|^2$ associated with $n \ge 1$ can also approximately resemble the node pattern of a bare Morse oscillator with the appropriate number of excitations, for small values of g/ω_{10}. For example, according to what was said, $|\Psi_6\rangle$ should have components in the uncoupled basis $|v\rangle|n\rangle$ such that $v + n = 3$ at zero detuning ($\omega_c = \omega_{10}$). For $g/\omega_{10} = 0.1$, Fig. 6 shows that indeed for $n = 1$ the nuclear density $|\Phi_{61}(q)|^2$ of state $|\Psi_6\rangle$ has a node structure similar to the bare Morse eigenstate $|v = 2\rangle$, i.e., it has two nodes. The nuclear densities associated with $n = 2$ and $n = 3$ also seem to satisfy a conservation rule for the total number of excitations ($v + n$). This rule however is broken for the $n = 4$ nuclear wave packet $\Phi_{64}(q)$ (Fig. 6, upper panel), which has a node structure similar to the bare Morse eigenstate $|v = 1\rangle$, corresponding to a total number of excitations $v + n = 5$.

In order to assess the contribution of each photon-number-dependent nuclear wave packet $\Phi_{jn}(q)$ on the jth polariton eigenstate $|\Psi_j\rangle$, we show in Fig. 7 the probability amplitudes $|c_{vn}|^2$ [see Eq. (16)] as a function of the coupling ratio g/ω_{10}, for the excited polariton eigenstates $|\Psi_6\rangle$ and $|\Psi_8\rangle$. These two excited states tend asymptotically to the energy $E \approx 3\ \omega_{10}$ as $g \to 0$ and therefore can be expected to be mainly composed of uncoupled states $|v\rangle|n\rangle$ such that $v + n = 3$,

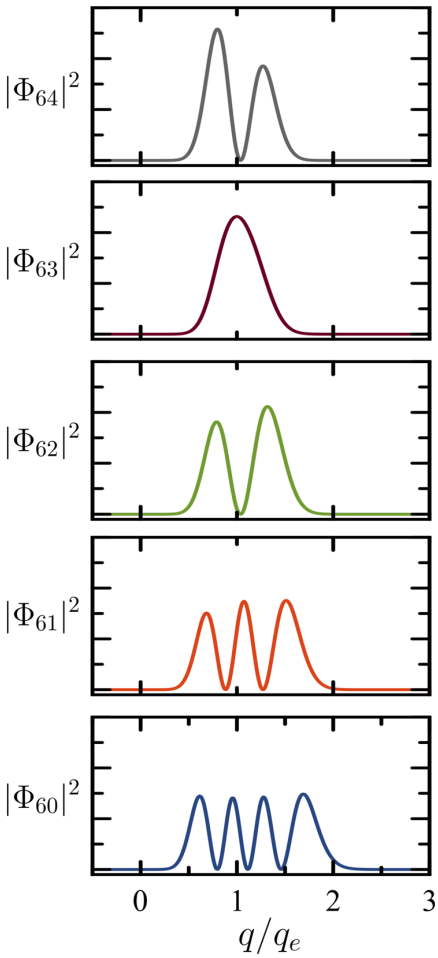

FIG. 6. Conditional probability densities $|\Phi_{6n}(q)|^2$ for the excited polariton eigenstate $|\Psi_6\rangle$, for coupling strength $g/\omega_{10} = 0.1$. Coordinates are in units of the bare equilibrium bond length q_e. All densities are normalized.

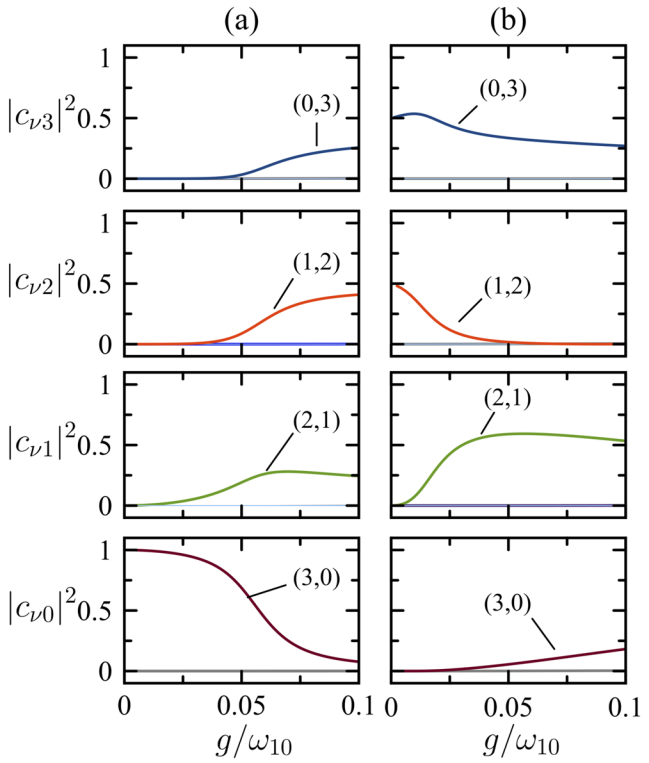

FIG. 7. Probability amplitudes $|c_{\nu n}|^2$ in the uncoupled basis $|\nu\rangle|n\rangle$ for excited polariton eigenstates $|\Psi_6\rangle$ (a) and $|\Psi_8\rangle$ (b), as a function the coupling strength g/ω_{10}. Curves are labeled by the quantum numbers (ν, n). We set $\omega_c = \omega_{10}$.

for resonant coupling. Figure 7 shows that this indeed occurs for $g/\omega_{10} \ll 1$. In this small coupling regime, the selected polariton eigenstates can be approximately written in the basis $|\nu\rangle|n\rangle$ as

$$|\Psi_6\rangle \approx |3\rangle|0\rangle \tag{19}$$

and

$$|\Psi_8\rangle \approx a|0\rangle|3\rangle + b|1\rangle|2\rangle, \tag{20}$$

where $|a|^2 \approx |b|^2 = 0.5$. As the coupling strength reaches the regime $g/\omega_{10} \sim 0.1$, the near resonant coupling between vibrational manifolds with higher photon numbers in Fig. 4 leads to the emergence of wavefunction components with lower vibrational quantum numbers. For instance, for $g/\omega_{10} = 0.1$, the excited state $|\Psi_6\rangle$ is approximately given by

$$|\Psi_6\rangle \approx a|1\rangle|2\rangle + b|0\rangle|3\rangle + c|2\rangle|1\rangle + d|1\rangle|4\rangle, \tag{21}$$

where $|a|^2 \sim |b|^2 > |c|^2 \gg |d|^2$. In other words, the state evolves from a bare Morse oscillator $|\nu = 3\rangle$ in vacuum [see Eq. (19)], into a state with a lower mean vibrational excitation and higher mean photon number as g/ω_{10} grows. On the other hand, the state $|\Psi_8\rangle$ at $g/\omega_{10} = 0.1$ can be written as

$$|\Psi_8\rangle \approx a|3\rangle|0\rangle + b|2\rangle|1\rangle + c|0\rangle|3\rangle + d|1\rangle|4\rangle, \tag{22}$$

where $|a|^2 \approx 1/2 > |b|^2 > |c|^2 \gg |d|^2$, which also develops components with lower vibrational quanta and higher photon numbers in comparison with Eq. (20). The emergence of uncoupled components with $\nu + n \neq 3$ in Eqs. (21) and (22) is a consequence of the counter-rotating terms in Eq. (11). Although the results in Figs. 6 and 7 were obtained for specific polariton eigenstates, we find that they qualitatively describe the behavior of most excited polaritons $|\Psi_j\rangle$ with energies $E_j \gg \omega_{10}$, i.e., above the LP and UP frequency regions.

We can also understand the structure of vibrational polaritons in coordinate space and Fock space by analyzing the dependence of the mean bond distance $\langle\hat{q}\rangle$ and the mean photon number $\langle\hat{a}^\dagger\hat{a}\rangle$ with the coupling parameter g and cavity detuning Δ, for selected polariton eigenstates. In Fig. 8, we compare the dependence of these observables on g and Δ for the system ground state $|\Psi_0\rangle$ (GS), the lower polariton state $|\Psi_1\rangle$, and the upper polariton state $|\Psi_2\rangle$. In the

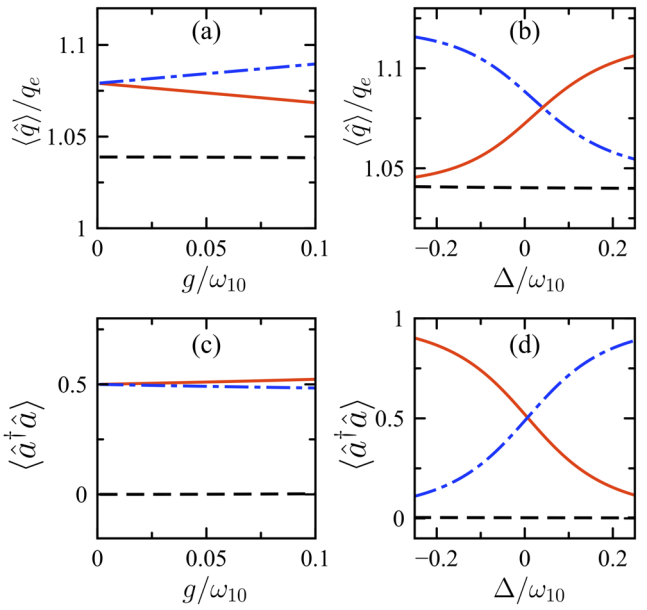

FIG. 8. Mean bond length $\langle\hat{q}\rangle$ and mean cavity photon number $\langle\hat{a}^\dagger\hat{a}\rangle$ as a function of coupling strength g/ω_{10} [(a) and (c)] and cavity detuning Δ [(b) and (d)], for the system ground state (dashed line), lower polariton (solid line), and upper polariton (dotted-dashed line). We set $\Delta = 0$ in panels (a) and (c) and $g/\omega_{10} = 0.1$ in panels (b) and (d). Energy is in units of ω_{10}.

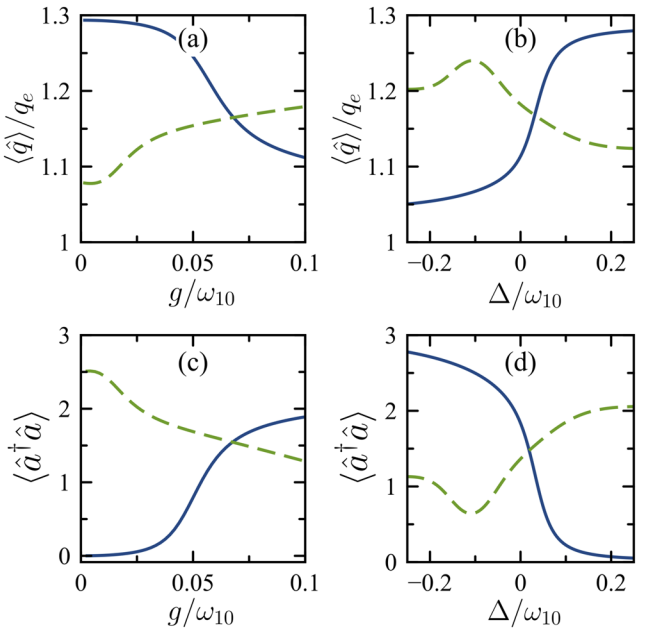

FIG. 9. Mean bond length $\langle\hat{q}\rangle$ and mean cavity photon number $\langle\hat{a}^\dagger\hat{a}\rangle$ as a function of coupling strength g/ω_{10} [(a) and (c)] and cavity detuning Δ [(b) and (d)], for excited polaritons $|\Psi_6\rangle$ (solid line) and $|\Psi_8\rangle$ (dashed line). We set $\Delta = 0$ in panels (a) and (c) and $g/\omega_{10} = 0.1$ in panels (b) and (d). Energy is in units of ω_{10}.

regime $g/\omega_{10} \ll 1$, both LP and UP have approximately the same bond length, given by

$$\langle\hat{q}\rangle \approx \frac{1}{2}(\langle 0|\hat{q}|0\rangle + \langle 1|\hat{q}|1\rangle), \tag{23}$$

with the expectation value taken with respect to Morse eigenstates $|v\rangle$.

Figure 8(a) shows that as the coupling strength increases, the bond length of the LP $\langle\hat{q}\rangle_{LP}$ decreases whilst $\langle\hat{q}\rangle_{UP}$ grows. The value of $\langle\hat{q}\rangle$ for the UP is upper bounded by the bond length of the first excited Morse state $|v = 1\rangle$. Considering that the bond distance is inversely related to its strength, for resonant coupling the molecular bond in the LP state becomes stronger relative to the UP with increasing coupling strength, although both polariton states experience bond strengthening in comparison with the Morse eigenstate $|v = 1\rangle$, which is in the same energy region as LP and UP ($E/\omega_{10} \approx 1$).

Bond strengthening should be accompanied by the creation of virtual cavity photons and bond softening by the decrease in the mean photon number. Figure 8(b) shows that the GS, LP, and UP states follow this behavior as a function of g/ω_{10}, for resonant coupling. We show in panels 8 (b) and (d) that for detuned cavities, the compromise between bond strength and cavity photon occupation also holds. Within the range of system parameters considered, we find that this compromise also holds for higher excited vibrational polaritons, as Fig. 9 shows for states $|\Psi_6\rangle$ and $|\Psi_8\rangle$.

Bond strengthening of vibrational polaritons can be understood by recalling that an eigenstate $|\Psi_j\rangle$ in the vicinity of a bare Morse energy level $E_{v'}$ in general has nonvanishing components in the uncoupled basis $|v\rangle|n\rangle$ with $v < v'$ [see Eq. (16)]. These low-v components contribute to the stabilization of the molecular bond even at high excitation energies.

VI. ENERGY CROSSINGS IN THE EXCITED POLARITON MANIFOLD

We discussed in Sec. III how the density of polariton levels increases with energy, ultimately due to the large number of near-degenerate uncoupled subspaces $|v\rangle|n\rangle$ (see Fig. 4). Light-matter coupling leads to the formation of closely spaced polariton levels that can become quasidegenerate at specific values of g and Δ. As the Hamiltonian parameters (g, Δ) are tuned across the degeneracy point, the polariton levels may undergo true or avoided crossing. For a Hamiltonian like the quantum Rabi model for the qubit[57,58,61] and its multilevel generalizations,[62] parity is a conserved quantity. Therefore, polaritons in the quantum Rabi model have well-defined parity and level crossings are analyzed in the usual way: states with opposite parity undergo true crossing under variation of a Hamiltonian parameter. In particular, the crossing of the ground state with the lower polariton state at $g/\omega_c = 1$ marks the onset of the deep strong coupling regime of the quantum Rabi model.[31,63,64]

Parity conservation in the quantum Rabi model ultimately emerges from the even character of the underlying microscopic Hamiltonians that describe the material system and the cavity field. The harmonic oscillator Hamiltonian that describes the cavity field is invariant under the transformation $\hat{a} \to -\hat{a}$ and therefore commutes with parity, as expected. For the molecular system, let $\hat{q}$ and $\hat{p}$

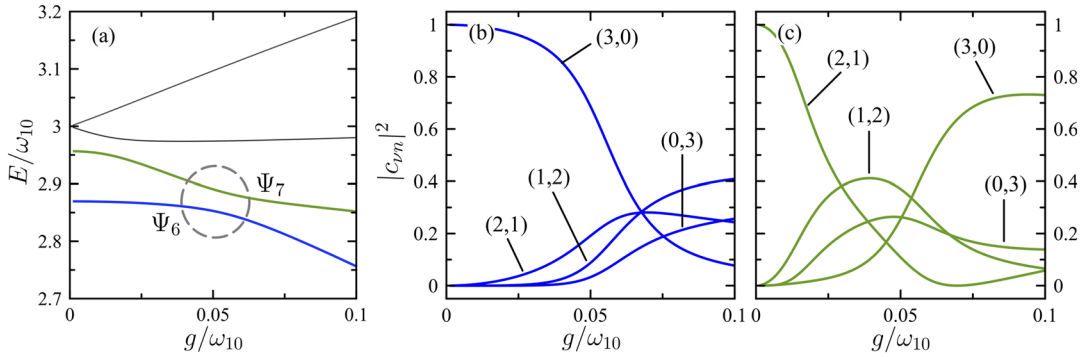

FIG. 10. (a) Spectral region with an avoided crossing (circled in gray) involving the excited polaritons $|\Psi_6\rangle$ (blue) and $|\Psi_7\rangle$ (green). [(b) and (c)] Main components of $|\Psi_6\rangle$ and $|\Psi_7\rangle$, respectively, in the uncoupled basis $|v\rangle|n\rangle$. Curves are labeled by the quantum numbers (v, n). We set $\omega_c = \omega_{10}$.

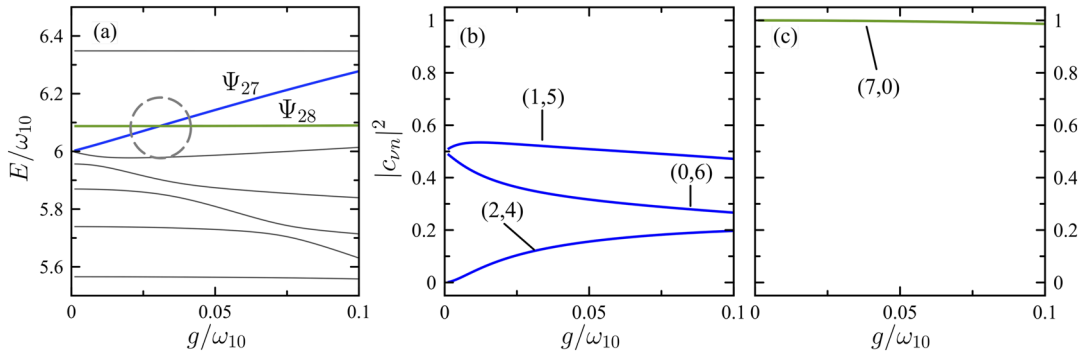

FIG. 11. (a) Spectral region with a true crossing (circled in gray) involving the excited polaritons $|\Psi_{27}\rangle$ (blue) and $|\Psi_{28}\rangle$ (green). [(b) and (c)] Main components of $|\Psi_{27}\rangle$ and $|\Psi_{28}\rangle$, respectively, in the uncoupled basis $|v\rangle|n\rangle$. Curves are labeled by the quantum numbers (v, n). We set $\omega_c = \omega_{10}$.

represent position and momentum operators in the material Hamiltonian $\hat{H}_{\rm M}$. Then, polariton eigenstates of the coupled light-matter system would only have well-defined parity if $\hat{H}_{\rm M}$ is invariant under the parity transformation $\hat{q} \to -\hat{q}$ and $\hat{p} \to -\hat{p}$. The Morse potential in Eq. (1) is not invariant under the transformation $q \to -q$ and $q_e \to -q_e$ and therefore breaks the parity of the material system. This is the origin of vibrational overtone transitions with $|\Delta v| \geq 2$. Therefore, polariton eigenstates of the MLQR model are not eigenstates of parity.

Even when vibrational polaritons do not have well-defined parity, the spectrum exhibits true and avoided level crossings as the Hamiltonian parameters g and Δ vary. We can track the origin of these crossings into an effective photonic parity selection rule imposed by the light-matter interaction term in the total Hamiltonian [Eq. (11)], which reads $\Delta n = \pm 1$. For two near-degenerate polariton levels E_j and E_k $(k \neq j)$, there will be a strong avoided crossing between them only if the largest probability amplitudes c_{vn} of their wavefunctions $|\Psi_j\rangle$ and $|\Psi_k\rangle$ in the uncoupled basis $|v\rangle|n\rangle$ differ by one photon number [see Eq. (16)]. Otherwise, the levels will cross as the Hamiltonian is varied through the degeneracy. We show this explicitly in Figs. 10 and 11, with examples of avoided and true crossings, respectively, in the excited polariton manifold.

In Fig. 10(a), we highlight an avoided crossing between excited polaritons $|\Psi_6\rangle$ and $|\Psi_7\rangle$ near $g/\omega_{10} \approx 0.05$. Panels 10(b) and 10(c) show that the largest wavefunction components to the left of the avoided crossing are $\{|3\rangle|0\rangle, |2\rangle|1\rangle\}$ for $|\Psi_6\rangle$ and $\{|1\rangle|2\rangle, |0\rangle|3\rangle |2\rangle|1\rangle\}$ for $|\Psi_7\rangle$, which indeed differ by one photon number. Past the avoided crossing, the state $|\Psi_7\rangle$ dominantly acquires $|3\rangle|0\rangle$ character.

In Fig. 11(a), we highlight a level crossing at $g/\omega_{10} \simeq 0.03$, where the excited polariton states $|\Psi_{27}\rangle$ and $|\Psi_{28}\rangle$ undergo a true crossing. Figure 11(b) shows that to the left of the crossing point, the largest uncoupled components of $|\Psi_{27}\rangle$ are $\{|1\rangle|5\rangle, |0\rangle|6\rangle\}$, while for $|\Psi_{28}\rangle$ the largest components are $\{|7\rangle|0\rangle\}$. Since $|\Psi_{27}\rangle$ and $|\Psi_{28}\rangle$ thus predominantly satisfy $\Delta n > 1$, they do not interact via by the light-matter term as g is varied across the degeneracy.

VII. CONCLUSION AND OUTLOOK

In order to understand the microscopic behavior of an individual anharmonic molecular vibration coupled to a single infrared cavity mode, we introduce and analyze the multilevel quantum Rabi (MLQR) model of vibrational polaritons [Eq. (11)]. We derive the model Hamiltonian starting from the exact anharmonic solutions of a free-space Morse oscillator and treat light-matter

interaction within the Power-Zineau-Woolley multipolar framework,[50] which includes the dipole self-energy. The model takes into account counter-rotating terms in the light-matter coupling and allows the analysis of vibrational polaritons both in Hilbert space and nuclear coordinate space. Phase-space representations of the photon state follow directly from the QED formulation of the model.[65] Such phase-space analysis would be closely related to previous coordinate-only treatments of photon-nuclei coupling,[28,39,66] although a systematic comparison has yet to be done.

The model is consistent with previous work based on few-level vibrational systems[38] and therefore is also able to describe the spectral features observed in linear and nonlinear transmission spectroscopy,[26,41] which, due to the relatively weak intensities involved, can only probe up to the second excited polariton triplet around $E \approx 2\ \omega_{10}$, where ω_{10} is the fundamental vibration frequency. The system Hamiltonian allows the emergence of an ensemble of avoided and true crossings as the Rabi frequency g and cavity detuning Δ are tuned. The density of these level crossings increases with energy. These crossings are governed by a pseudoparity selection rule in the photonic degree of freedom (details in Sec. V).

The nuclear coordinate analysis of vibrational polaritons within the MLQR model unveils a few general trends across the entire energy spectrum. First, it is no longer possible to define a unique bond dissociation energy in an infrared cavity as is commonly done in free space. The dissociation energy depends on the quantum state of the cavity field. Second, within any given energy range ΔE, it is always possible to find a vibrational polariton eigenstate with small mean photon number $\langle \hat{a}^\dagger \hat{a} \rangle$ and large mean bond distance $\langle \hat{q} \rangle$, and vice-versa. Third, the bond distance $\langle \hat{q} \rangle$ of an arbitrary vibrational polariton state with energy, E_j, never exceeds the bond length of a free-space Morse eigenstate $|v\rangle$ with similar energy ($E_v \approx E_j$). In other words, the formation of vibrational polaritons inside the cavity leads to a type of *bond-strengthening* effect that may have consequences in the reactivity of chemical bonds.

The multilevel quantum Rabi model developed here can be generalized to the many-molecule and multimode scenarios. Treating the dissipative dynamics of vibrational polaritons due to cavity photon decay and vibrational relaxation is also straightforward within a Markovian approach.[67] The dynamics of vibrational polaritons in the many-body regime has been previously discussed in Refs. 33 and 68, using truncated vibrational subspaces. The main qualitatively new effect that the many-body system introduces to the problem is the formation of collective molecular states that are not symmetric with respect to particle permutations. These so-called "dark exciton states"[69] arise naturally from state classification by permutation symmetry in the Hilbert space of the Dicke model.[70,71] It has been shown originally within a quasiparticle approach for systems with macroscopic translational invariance,[72] and later using a cavity QED approach,[32,73,74] that totally symmetric and nonsymmetric collective molecular states can strongly admix due to the ever-present inhomogeneous broadening of molecular energy levels, by inhomogeneities in the light-matter interaction energy across the medium or by any local coherent term such as intramolecular electron-vibration coupling (in the case of electronic strong coupling[74]). For the case of vibrational polaritons, the role of dark and quasidark collective states in determining the rate of chemical reactions is yet to be fully understood.

SUPPLEMENTARY MATERIAL

In the supplementary material, we show the dependence of the energy spectrum, mean bond length, and mean photon number of vibrational polaritons on the value of the anharmonicity parameter χ_e with fixed dissociation energy D_e.

ACKNOWLEDGMENTS

We thank Guillermo Romero, Blake Simpkins, and Jeffrey Owrutsky for discussions. We are thankful for the support from CONICYT through the Proyecto REDES ETAPA INICIAL, Convocatoria 2017 No. REDI 170423, and FONDECYT Regular No. 1181743, and are also thankful for the support from Iniciativa Cientifica Milenio (ICM) through the Millennium Institute for Research in Optics (MIRO).

REFERENCES

[1] H. J. Kimble, "The quantum internet," Nature **453**(7198), 1023 (2008).
[2] J. L. O'Brien, A. Furusawa, and J. Vučković, "Photonic quantum technologies," Nat. Photonics **3**(12), 687–695 (2009).
[3] H. Mabuchi and A. C. Doherty, "Cavity quantum electrodynamics: Coherence in context," Science **298**(5597), 1372–1377 (2002).
[4] A. Blais, R.-S. Huang, A. Wallraff, S. M. Girvin, and R. J. Schoelkopf, "Cavity quantum electrodynamics for superconducting electrical circuits: An architecture for quantum computation," Phys. Rev. A **69**, 062320 (2004).
[5] R. Miller *et al.*, "Trapped atoms in cavity QED: Coupling quantized light and matter," J. Phys. B: At., Mol. Opt. Phys. **38**(9), S551 (2005).
[6] T. W. Ebbesen, "Hybrid light-matter states in a molecular and material science perspective," Acc. Chem. Res. **49**, 2403–2412 (2016).
[7] A. Canaguier-Durand, E. Devaux, J. George, Y. Pang, J. A. Hutchison, T. schwartz, C. Genet, N. Wilhelms, J.-M. Lehn, and T. W. Ebbesen, "Thermodynamics of molecules strongly coupled to the vacuum field," Angew. Chem., Int. Ed. **52**(40), 10533–10536 (2013).
[8] J. P. Long and B. S. Simpkins, "Coherent coupling between a molecular vibration and Fabry–Perot optical cavity to give hybridized states in the strong coupling limit," ACS Photonics **2**(1), 130–136 (2015).
[9] B. S. Simpkins, K. P. Fears, W. J. Dressick, B. T. Spann, A. D. Dunkelberger, and J. C. Owrutsky, "Spanning strong to weak normal mode coupling between vibrational and Fabry–Pérot cavity modes through tuning of vibrational absorption strength," ACS Photonics **2**(10), 1460–1467 (2015).
[10] A. Shalabney, J. George, H. Hiura, and J. A. Hutchison, C. Genet, P. Hellwig, and T. W. Ebbesen, "Enhanced Raman scattering from vibro-polariton hybrid states," Angew. Chem., Int. Ed. **54**(27), 7971–7975 (2015).
[11] A. Shalabney, J. George, J. Hutchison, G. Pupillo, C. Genet, and T. W. Ebbesen, "Coherent coupling of molecular resonators with a microcavity mode," Nat. Commun. **6**, 5981 (2015).
[12] R. Chikkaraddy, B. de Nijs, F. Benz, S. J. Barrow, O. A. Scherman, E. Rosta, A. Demetriadou, P. Fox, O. Hess, and J. J. Baumberg, "Single-molecule strong coupling at room temperature in plasmonic nanocavities," Nature **535**(7610), 127–130 (2016).
[13] F. Benz, M. K. Schmidt, A. Dreismann, R. Chikkaraddy, Y. Zhang, A. Demetriadou, C. Carnegie, H. Ohadi, B. de Nijs, R. Esteban, J. Aizpurua, and J. J. Baumberg, "Single-molecule optomechanics in picocavities," Science **354**(6313), 726–729 (2016).
[14] J. George, T. Chervy, A. Shalabney, E. Devaux, H. Hiura, C. Genet, and T. W. Ebbesen, "Multiple Rabi splittings under ultrastrong vibrational coupling," Phys. Rev. Lett. **117**(15), 153601 (2016).
[15] R. M. A. Vergauwe, J. George, T. Chervy, J. A. Hutchison, A. Shalabney, V. Y. Torbeev, and T. W. Ebbesen, "Quantum strong coupling with protein vibrational modes," J. Phys. Chem. Lett. **7**(20), 4159–4164 (2016).

[16]A. Thomas, J. George, A. Shalabney, M. Dryzhakov, J. Sreejith, J. M. Varma, T. Chervy, X. Zhong, E. Devaux, C. Genet, and J. A. Hutchison, and T. W. Ebbesen, "Ground-state chemical reactivity under vibrational coupling to the vacuum electromagnetic field," Angew. Chem., Int. Ed. **55**(38), 11462–11466 (2016).
[17]M. Hertzog, P. Rudquist, J. A. Hutchison, J. George, T. W. Ebbesen, and K. Börjesson, "Voltage-controlled switching of strong light-matter interactions using liquid crystals," Chem. - Eur. J. **23**(72), 18166–18170 (2017).
[18]D. Wang, H. Kelkar, D. Martin-Cano, T. Utikal, S. Götzinger, and V. Sandoghdar, "Coherent coupling of a single molecule to a scanning Fabry-Perot microcavity," Phys. Rev. X **7**(2), 021014 (2017).
[19]V. F. Crum, S. R. Casey, and J. R. Sparks, "Photon-mediated hybridization of molecular vibrational states," Phys. Chem. Chem. Phys. **20**(2), 850–857 (2018).
[20]T. Chervy, A. Thomas, E. Akiki, R. M. A. Vergauwe, A. Shalabney, J. George, E. Devaux, J. A. Hutchison, C. Genet, and T. W. Ebbesen, "Vibro-polaritonic IR emission in the strong coupling regime," ACS Photonics **5**(1), 217–224 (2018).
[21]M. Du, R. F. Ribeiro, and J. Yuen-Zhou, "Remote control of chemistry in optical cavities," Chem **5**(5), 1167–1181 (2019).
[22]H. Hiura, A. Shalabney, and J. George, "Cavity catalysis ? accelerating reactions under vibrational strong coupling ?," chemRxiv (to be published).
[23]A. Thomas, L. Lethuillier-Karl, K. Nagarajan, R. M. A. Vergauwe, J. George, T. Chervy, A. Shalabney, E. Devaux, C. Genet, J. Moran, and T. W. Ebbesen, "Tilting a ground-state reactivity landscape by vibrational strong coupling," Science **363**(6427), 615–619 (2019).
[24]R. J. Gordon, L. Zhu, and T. Seideman, "Coherent control of chemical reactions," Acc. Chem. Res. **32**(12), 1007–1016 (1999).
[25]J. del Pino, J. Feist, and F. J. Garcia-Vidal, "Signatures of vibrational strong coupling in Raman scattering," J. Phys. Chem. C **119**(52), 29132–29137 (2015).
[26]A. D. Dunkelberger, B. T. Spann, K. P. Fears, B. S. Simpkins, and J. C. Owrutsky, "Modified relaxation dynamics and coherent energy exchange in coupled vibration-cavity polaritons," Nat. Commun. **7**, 1–10 (2016).
[27]A. D. Dunkelberger, R. B. Davidson II, W. Ahn, B. S. Simpkins, and J. C. Owrutsky, "Ultrafast transmission modulation and recovery via vibrational strong coupling," J. Phys. Chem. A **122**(4), 965–971 (2018).
[28]J. Feist, J. Galego, and F. J. Garcia-Vidal, "Polaritonic chemistry with organic molecules," ACS Photonics **5**(1), 205–216 (2018).
[29]R. F. Ribeiro, L. A. Martínez-Martínez, M. Du, J. Campos-Gonzalez-Angulo, and J. Yuen-Zhou, "Polariton chemistry: Controlling molecular dynamics with optical cavities," Chem. Sci. **9**(30), 6325–6339 (2018).
[30]M. Hertzog, M. Wang, J. Mony, and K. Börjesson, "Strong light–matter interactions: A new direction within chemistry," Chem. Soc. Rev. **48**(3), 937–961 (2019).
[31]A. F. Kockum, A. Miranowicz, S. De Liberato, S. Savasta, and F. Nori, "Ultrastrong coupling between light and matter," Nat. Rev. Phys. **1**, 19–40 (2019).
[32]F. Herrera and F. C. Spano, "Cavity-controlled chemistry in molecular ensembles," Phys. Rev. Lett. **116**, 238301 (2016).
[33]J. del Pino, J. Feist, and F. J. Garcia-Vidal, Quantum theory of collective strong coupling of molecular vibrations with a microcavity mode, New J. Phys. **17**, 053040 (2015).
[34]M. Muallem, A. Palatnik, G. D. Nessim, and Y. R. Tischler, "Strong light-matter coupling and hybridization of molecular vibrations in a low-loss infrared microcavity," J. Phys. Chem. Lett. **7**(11), 2002–2008 (2016).
[35]P. Saurabh and S. Mukamel, "Two-dimensional infrared spectroscopy of vibrational polaritons of molecules in an optical cavity," J. Chem. Phys. **144**(12) (2016).
[36]H. Ling Luk, J. Feist, J. Jussi Toppari, and G. Groenhof, "Multiscale molecular dynamics simulations of polaritonic chemistry," J. Chem. Theory Comput. **13**(9), 4324–4335 (2017).
[37]L. A. Martínez-Martínez, R. F. Ribeiro, J. Campos-González-Angulo, and J. Yuen-Zhou, "Can ultrastrong coupling change ground-state chemical reactions?," ACS Photonics **5**(1), 167–176 (2018).
[38]B. Xiang, W. Xiong, B. S. Simpkins, J. C. Owrutsky, R. F. Ribeiro, A. D. Dunkelberger, and J. Yuen-Zhou, "Theory for nonlinear spectroscopy of vibrational polaritons," J. Phys. Chem. Lett. **9**(13), 3766–3771 (2018).
[39]J. Flick, M. Ruggenthaler, H. Appel, and A. Rubio, "Atoms and molecules in cavities, from weak to strong coupling in quantum-electrodynamics (QED) chemistry," Proc. Natl. Acad. Sci. U. S. A. **114**(12), 3026–3034 (2017).
[40]J. Flick, H. Appel, M. Ruggenthaler, and A. Rubio, "Cavity Born-Oppenheimer approximation for correlated electron-nuclear-photon systems," J. Chem. Theory Comput. **13**(4), 1616–1625 (2017).
[41]B. Xiang, R. F. Ribeiro, A. D. Dunkelberger, J. Wang, Y. Li, B. S. Simpkins, J. C. Owrutsky, J. Yuen-Zhou, and W. Xiong, "Two-dimensional infrared spectroscopy of vibrational polaritons," Proc. Natl Acad. Sci. **115**(19), 4845–4850 (2018).
[42]P. M. Morse, "Diatomic molecules according to the wave mechanics. II. Vibrational levels," Phys. Rev. **34**(1), 57–64 (1929).
[43]V. S. Vasan and R. J. Cross, "Matrix elements for Morse oscillators," J. Chem. Phys. **78**(6), 3869–3871 (1983).
[44]J. C. Light and T. Carrington, Jr., *Discrete-Variable Representations and Their Utilization* (John Wiley & Sons, 2007), pp. 263–310.
[45]D. T. Colbert and W. H. Miller, "A novel discrete variable representation for quantum mechanical reactive scattering via the *S*-matrix Kohn method," J. Chem. Phys. **96**(3), 1982–1991 (1992).
[46]I. P. Hamilton and J. C. Light, "On distributed Gaussian bases for simple model multidimensional vibrational problems," J. Chem. Phys. **84**(1), 306–317 (1986).
[47]W. Demtröder, *Molecular Physics: Theoretical Principles and Experimental Methods* (John Wiley & Sons, 2008).
[48]P. Jakob and B. N. J. Persson, "Infrared spectroscopy of overtones and combination bands," J. Chem. Phys. **109**(19), 8641–8651 (1998).
[49]G. Marcus, A. Zigler, and L. Friedland, "Molecular vibrational ladder climbing using a sub-nanosecond chirped laser pulse," Europhys. Lett. **74**(1), 43–48 (2006).
[50]D. P. Craig and T. Thirunamachandran, *Molecular Quantum Electrodynamics: An Introduction to Radiation-Molecule Interactions* (Courier Corporation, 1998).
[51]D. L. Andrews, G. A. Jones, A. Salam, and R. G. Woolley, "Perspective: Quantum Hamiltonians for optical interactions," J. Chem. Phys. **148**(4), 040901 (2018).
[52]S. Y. Buhmann, *Dispersion Forces I: Macroscopic Quantum Electrodynamics and Ground-State Casimir, Casimir–Polder and van der Waals Forces*, Springer Tracts in Modern Physics (Springer Berlin Heidelberg, 2013).
[53]V. Rokaj, D. M. Welakuh, M. Ruggenthaler, and A. Rubio, "Light–matter interaction in the long-wavelength limit: No ground-state without dipole self-energy," J. Phys. B: At., Mol. Opt. Phys. **51**(3), 034005 (2018).
[54]A. I. Burshtein and S. I. Temkin, *Spectroscopy of Molecular Rotation in Gases and Liquids* (Cambridge University Press, 2005).
[55]L. Novotny and B. Hecht, *Principles of Nano-Optics* (Cambridge University Press, 2012).
[56]T. Werlang, A. V. Dodonov, E. I. Duzzioni, and C. J. Villas-Bôas, "Rabi model beyond the rotating-wave approximation: Generation of photons from vacuum through decoherence," Phys. Rev. A **78**, 053805 (2008).
[57]D. Braak, "Integrability of the Rabi model," Phys. Rev. Lett. **107**, 100401 (2011).
[58]F. A. Wolf, F. Vallone, G. Romero, M. Kollar, E. Solano, and D. Braak, "Dynamical correlation functions and the quantum Rabi model," Phys. Rev. A **87**, 023835 (2013).
[59]E. T. Jaynes and F. W. Cummings, "Comparison of quantum and semiclassical radiation theories with application to the beam maser," Proc. IEEE **51**(1), 89–109 (1963).
[60]O. Kühn, J. Manz, and Y. Zhao, "Ultrafast IR laser control of photodissociation: Single- vs. multi-pulse schemes," Phys. Chem. Chem. Phys. **1**, 3103–3110 (1999).
[61]Q.-H. Chen, C. Wang, S. He, T. Liu, and K.-L. Wang, "Exact solvability of the quantum Rabi model using Bogoliubov operators," Phys. Rev. A **86**, 023822 (2012).
[62]V. V. Albert, "Quantum Rabi model for *N*-state atoms," Phys. Rev. Lett. **108**, 180401 (2012).
[63]J. Casanova, G. Romero, I. Lizuain, J. J. García-Ripoll, and E. Solano, "Deep strong coupling regime of the Jaynes-Cummings model," Phys. Rev. Lett. **105**, 263603 (2010).

[64]P. Forn-Díaz, L. Lamata, E. Rico, J. Kono, and E. Solano, "Ultrastrong coupling regimes of light-matter interaction," Rev. Mod. Phys. **91**, 025005 (2019).
[65]H. Carmichael, *Statistical Mehods in Quantum Optics 1: Master Equations and Fokker-Planck Equations* (Springer Berlin, Heidelberg, 1999).
[66]J. F. Triana, D. Peláez, and J. L. Sanz-Vicario, "Entangled photonic-nuclear molecular dynamics of LiF in quantum optical cavities," J. Phys. Chem. A **122**(8), 2266–2278 (2018).
[67]H. P. Breuer and F. Petruccione, *The Theory of Open Quantum Systems* (Oxford University Press, 2002).
[68]A. Strashko and J. Keeling, "Raman scattering with strongly coupled vibron-polaritons," Phys. Rev. A **94**, 023843 (2016).
[69]M. Litinskaya, P. Reineker, and V. M. Agranovich. Fast polariton relaxation in strongly coupled organic microcavities. J. Lumin. **110**, 364–372 (2004).
[70]B. M. Garraway, "The Dicke model in quantum optics: Dicke model revisited," Philos. Trans. R. Soc., A **369**(1939), 1137–1155 (2011).
[71]P. Kirton, M. M. Roses, J. Keeling, and E. G. Dalla Torre, "Introduction to the Dicke model: From equilibrium to nonequilibrium, and vice versa," Adv. Quantum Tech. **2**(1-2), 1800043 (2019).
[72]M. Litinskaya and P. Reineker, "Loss of coherence of exciton polaritons in inhomogeneous organic microcavities," Phys. Rev. B **74**, 165320 (2006).
[73]F. Herrera and F. C. Spano, "Absorption and photoluminescence in organic cavity QED," Phys. Rev. A **95**, 053867 (2017).
[74]F. Herrera and F. C. Spano, "Theory of nanoscale organic cavities: The essential role of vibration-photon dressed states," ACS Photonics **5**, 65–79 (2018).